12-2001

Pulmonary Arterial Morphometry from Microfocal X-Ray Computed Tomography

Kelly L. Karau
College of Wisconsin

Robert C. Molthen
Marquette University, robert.molthen@marquette.edu

Anita H. Dhyani
Marquette

Steven Thomas Haworth
Marquette University

Christopher C. Hanger
Medical College of Wisconsin

See next page for additional authors

American Journal of Physiology : Heart and Circulatory Physiology, Vol. 281, No. 6 (2001): H2747-H2756. DOI.

Pulmonary Arterial Morphometry from Microfocal X-ray Computed Tomography

Kelly L. Karau
Department of Physiology and Department of Biomedical Engineering, Marquette University, Milwaukee
Robert C. Molthen
Departments of Physiology and Department of Biomedical Engineering, Marquette University, Milwaukee 53201; and Research Service, Zablocki Veterans Affairs Medical Center, Milwaukee, Wisconsin
Anita Dhyani
Department of Biomedical Engineering, Marquette University, Milwaukee
Steven T. Haworth
Department of Physiology, Medical College of Wisconsin
Christopher C. Hanger
Anesthesiology, Medical College of Wisconsin
David L. Roerig

Anesthesiology, Medical College of Wisconsin; Research Service, Zablocki Veterans Affairs Medical Center, Milwaukee, Wisconsin

Rodger H. Johnson

Department of Biomedical Engineering, Marquette University, Milwaukee

Christopher A. Dawson

Department of Physiology and Department of Biomedical Engineering, Marquette University, Milwaukee
Research Service, Zablocki Veterans Affairs Medical Center, Milwaukee, Wisconsin

Abstract

The objective of this study was to develop an X-ray computed tomographic method for pulmonary arterial morphometry. The lungs were removed from a rat, and the pulmonary arterial tree was filled with perfluorooctyl bromide to enhance X-ray absorbance. At each of four pulmonary arterial pressures (30, 21, 12, and 5.4 mmHg), the lungs were rotated within the cone of the X-ray beam that was projected from a microfocal X-ray source onto an image intensifier, and 360 images were obtained at 1° increments. The three-dimensional image volumes were reconstructed with isotropic resolution with the use of a cone beam reconstruction algorithm. The luminal diameter and distance from the inlet artery were measured for the main trunk, its immediate branches, and several minor trunks. These data revealed a self-consistent tree structure wherein the portion of the tree downstream from any vessel of a given diameter has a similar structure. Self-consistency allows the entire tree structure to be characterized by measuring the dimensions of only the vessels comprising the main trunk of the tree and its immediate branches. An approach for taking advantage of this property to parameterize the morphometry and distensibility of the pulmonary arterial tree is developed.

the extant luminal morphometry of the pulmonary arterial tree comes almost exclusively from measurements on plastic corrosion casts. That approach has been important in developing present concepts regarding pulmonary structure-function relationships. However, the data collection process is quite tedious, and, as a consequence, the data obtained to date are from very few lungs, i.e., usually from only one or two ostensibly normal lungs of each species that has been studied (13, 16, 18,33, 40). The laborious casting approach virtually precludes accumulation of data on the progression of the pulmonary arterial architecture during development or resulting from vascular remodeling associated with adaptation to physiological or pathophysiological stresses.

As an alternative to corrosion casting, X-ray computed tomography (CT) has the potential for increasing the throughput enough to make such studies practical (20, 21). The approach has been initiated in studies both in vivo (11, 24, 25) and in excised lungs (21, 38). Key advantages include the fact that the data set, including all the vessels with their spatial orientation and connectivity, is rapidly available in digitized form and that the data can be collected on the same lung under different experimental conditions (21).

However, the problems of quantifying the complex structure and then providing a useful quantitative summary of the large data set remain for both imaging and casting methods. One aspect of this problem is that there is no fully automated image segmentation method that provides the necessary accuracy and precision. Thus, as with casting methods, some subset of the data obtained with semiautomated methods must be used to extrapolate to the whole.

Various approaches have been developed for summarizing complex vascular morphometric data sets (3, 5, 6, 13, 14, 18). They vary in applicability to CT images and in the information content of the resulting summary. In the present study, we develop an approach for parameterizing the rat pulmonary arterial tree structure and vessel distensibility from X-ray CT images. The objective is a parameter vector useful for evaluating the efficacy of interventions directed at putative mechanisms of pulmonary vascular remodeling, as a quantitative trait vector for identifying genes involved in pulmonary vascular remodeling (7, 27), and as input to

mathematical models relating pulmonary vascular structure and function (5, 6,42). The approach is based on the concept of "self-consistency," as applied by Fredberg and Hoenig (9,10) to the bronchial tree. In this context, the definition of a self-consistent arterial tree is one in which all portions of the tree downstream from a vessel of a given diameter are, in a statistical sense, similar. That is, any artery of a given diameter subtends a similar number of terminal arterioles with a similar connecting network. One attribute of the self-consistent tree structure is that it can be fully characterized by measuring the dimensions of only the vessels that make up the main trunk of the tree and its immediate branches, where the main trunk is the route followed from the inlet pulmonary artery by taking the largest diameter branch at each successive bifurcation. In what follows we develop the rationale for parameterizing the rat arterial tree, referred to as a "principle pathway" analysis, based on measurements of the diameters and distances from the inlet of the main trunk and its immediate branches.

METHODS

Animal preparation.

The lung from a 320-g fawn-hooded rat, acclimated to the normal atmosphere at 193 m above sea level, was prepared for imaging as previously described (21). The rat was anesthetized with pentobarbital sodium (40 μg/g body wt ip), the trachea was clamped, and the chest was opened. Heparin sodium (200 IU in 0.2 ml) was administered via injection into the right ventricle. The pulmonary artery was cannulated with a saline-filled catheter of polyethylene tubing (1.67 mm inner diameter and 2.42 mm outer diameter) via the conus arteriosis, and the heart was dissected away. The lung was removed from the chest and suspended from the trachea and pulmonary arterial cannula. The lung was ventilated with 15% O_2-6% CO_2, balance nitrogen, at 40 breaths/min with end-inspiratory and end-expiratory tracheal pressures of 8 and 3 mmHg, respectively. This served to eliminate any atelectasis that may have occurred during the dissection. The pulmonary artery cannula was connected to a perfusion system primed with a physiological salt solution containing 5% bovine serum albumin, and the lung was perfused for ~5 min at a flow rate in the range of 5–40 ml/min to remove residual blood from the lung vessels. The perfusate exited via the severed pulmonary vein. Once cleared of blood, the lung, still suspended from the cannulas, was placed in a 41-mm inner diameter plastic cylinder. The cylinder axis was located at the center of a horizontal turntable so that the lung could be rotated 360° around a vertical axis between the X-ray source and detector with no other significant X-ray absorbing objects passing through the beam. The airway pressure was set at 6 mmHg, and the solution in the reservoir connected to the arterial catheter was replaced by perfluorooctyl bromide (PFOB) that was allowed to fill the arterial tree at a pressure of ~20 mmHg. The PFOB provided high X-ray contrast for the vessel lumen, and the surface tension at the PFOB-aqueous interface prevented its entry into the capillary bed. Thus only the arterial vessels were filled. Then the arterial pressure was set at 30 mmHg relative to the horizontal plane through the center of the X-ray image of the lung. The lung was rotated and stopped at each 1° increment so that 360 X-ray images were acquired in ~10 min. The same sequence was repeated with the arterial pressure set at 21, 12, and 5.4 mmHg, respectively, and again at 30 mmHg. The actual intravascular pressure within each vessel relative to atmospheric pressure at the level of the vessel was obtained from the vertical distance of the vessel from the pressure reference level at the central horizontal plane of the image volume, and the PFOB density of 1.94 g/ml.

Imaging.

The X-ray system included an X-ray tube (model FXE-100.50; Fein-Focus) with a 3 μm focal spot, an image train consisting of an image intensifier set at the 17.8-cm aperture (model AI-5830-HP; North American Imaging), and a charge-coupled device camera (model SMD 1M15, Silicon Mountain Design; Colorado Springs, CO). The cylinder containing the rat lung was placed in the scanner so that its central axis was 26.7 cm from the source. The source-to-image intensifier distance was 91.3 cm, yielding a geometric magnification of ~×3.4 and a half-

cone beam angle for the lung image of ~4°. Projection-image collection frequency was 30 frames/s with 30 consecutive frames averaged to create each stored image. After the lung imaging session, two additional images were obtained. One was a flood field image with the lung removed from the beam. The flood field image was used to correct for spatial variations in the X-ray beam intensity and/or image intensifier gain. The other image was of a phantom consisting of a uniform grid of stainless steel spheres used as previously described (21) to correct for spatial distortion (warping) inherent in the image intensifier.

Each of the 360, 8-bit planar images, consisting of a 512 × 512 array of pixels in the range of 0–255 (minimum to maximum) X-ray intensity scale, was preprocessed as previously described (21) to correct the image intensifier spatial distortion, to locate the axis of rotation, and to correct for nonuniform illumination intensity. After preprocessing, cone-beam reconstruction was performed on the projection data to yield an isotropic reconstruction matrix of 497 × 497 × 497 voxels representing a volume of ~3.8 × 3.8 × 3.8 cm^3. The Feldkamp (8, 19) cone-beam algorithm was utilized to account for the variation in the angle of the incident X-ray beam at each pixel in the projection images. A filtered [Shepp-Logan filter kernel (32)] backprojection reconstruction was then performed.

Measurements.

The three-dimensional (3D) surface-shaded renderings of the arterial tree in Figs. 1 and 2 help to demonstrate the concept behind the subsequent measurements made on the reconstructed image volume.
Figure 1*A* illustrates a rat lung image volume with the threshold set to eliminate the tissue and smallest vessels, which tend to obscure the pulmonary arterial tree structure viewed at this magnification. Figure 1*B* was obtained by electronically pruning the tree so that the main pathway, composed of the main trunk and the stumps of its immediate branches, is separated from the rest of the tree. Figure2 presents two views obtained after ligating the right pulmonary artery and physically removing the right lung before imaging. This was done to provide a less cluttered view of the smaller branches than in the whole lung image in Fig. 1. When this left lung image is rotated, so that a given small portion is close to being in the plane of the page, one can appreciate the self-consistent appearance by comparing the two circled portions. That is, one could imagine that swapping the positions of the two circled portions would hardly affect the overall tree structure.

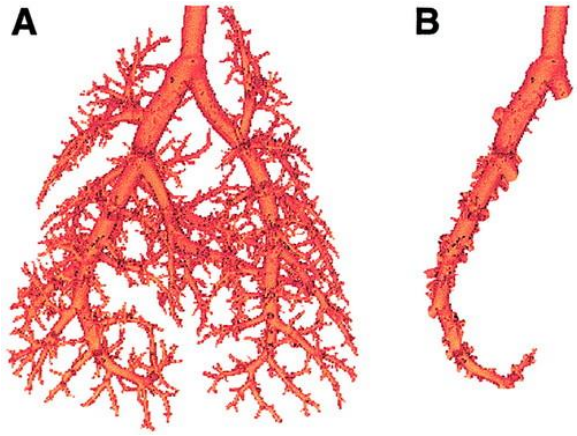

Fig. 1. *A*: surface-shaded rendering of the rat pulmonary arterial tree with the threshold chosen to obscure the smallest vessels to provide an uncluttered view of the overall structure. *B*: main trunk, with the stumps of its branches attached, was obtained by electronically pruning the image on the left. Measurements of diameter of the main trunk along its length and the positions and diameters of branches off of the main trunk compose the principal pathway data set.

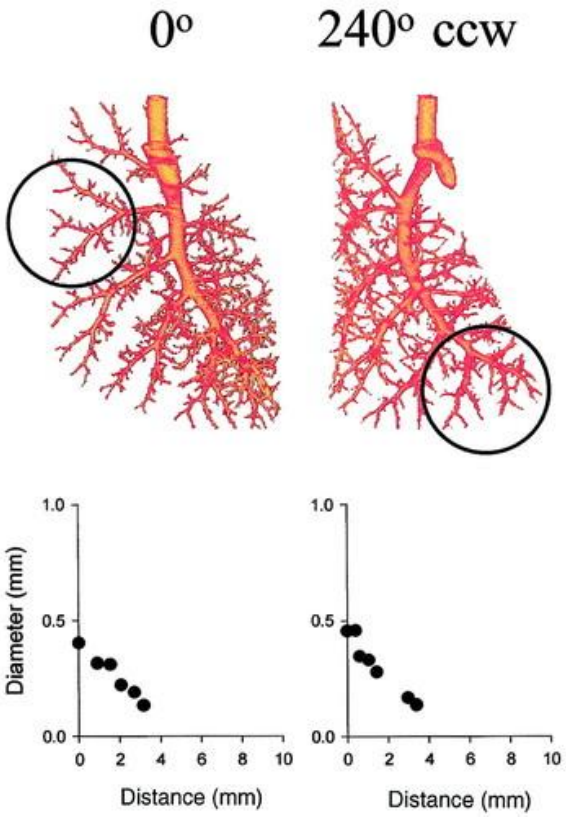

Fig. 2. Surface-shaded renderings after ligating the right pulmonary artery and physically removing the right lung before imaging. This was done to provide a less cluttered view of the smaller branches than in the whole lung image in Fig. 1. When this left lung image is rotated so that a given small portion is close to being in the plane of the page, one can appreciate the self-consistent appearance exemplified by two circled portions. The graphs below the two images are of the diameter vs. distance along the trunk within the circle as a means of making a quantitative assessment of the similarity between the two regions. CCW, counterclockwise.

In what follows, the full data set, with no artificial threshold, was used to make quantitative measurements wherein the gray scale number (GSN), obtained from the reconstruction is the measure of X-ray absorption within a given voxel (21).

Mapping the principle pathway.

For this analysis, a trunk is a pathway through the tree defined by following the path of the largest diameter branch at each bifurcation. The main trunk is the trunk that starts at the main pulmonary artery. Because of the correlation between the distance between bifurcations and diameter, the main trunk is either the longest, or very nearly the longest, pathway through the tree. A minor trunk can start at any bifurcation. To begin the principal pathway analysis, several trunks were followed through transaxial slices of the three-dimensional volume from their respective inlets to their most distal resolved vessel segments. The first step in this process was to identify axial*x*,*y*,*z* coordinates along a trunk that could be used to specify locations for measuring trunk and branch diameters and their distances from the trunk inlet. These coordinates were identified interactively using an approach similar to that described previously (21) but with modification required to track a vessel regardless of its angle relative to the rotation axis of the image volume.

In the description of the method for identifying *x*,*y*,*z* coordinates, the terms trunk and branch can be interchanged. The only distinction is that downstream from a bifurcation the trunk has the larger of the two

diameters. In the most common case, the trunk and branch cross sections were oblique to the transaxial slices and the branch and trunk diverged on progression through the transaxial slices. This is shown diagrammatically by the trunk and *branch A* in Fig.3. In this case, a bifurcation was located by observing the trunk cross-section while progressing through the sequence of transaxial slices until the single ellipsoid became bilobular and then split into two. The slice number, in which there was visible separation between the two new ellipsoids (the crotch of the bifurcation), was taken as the *z* coordinate as depicted in Fig. 3 (gold-colored diamonds). The central *x,y* coordinates of each of the two ellipsoids on the slice at which the single ellipsoid completely separated into two, were recorded along with the*z* coordinate.

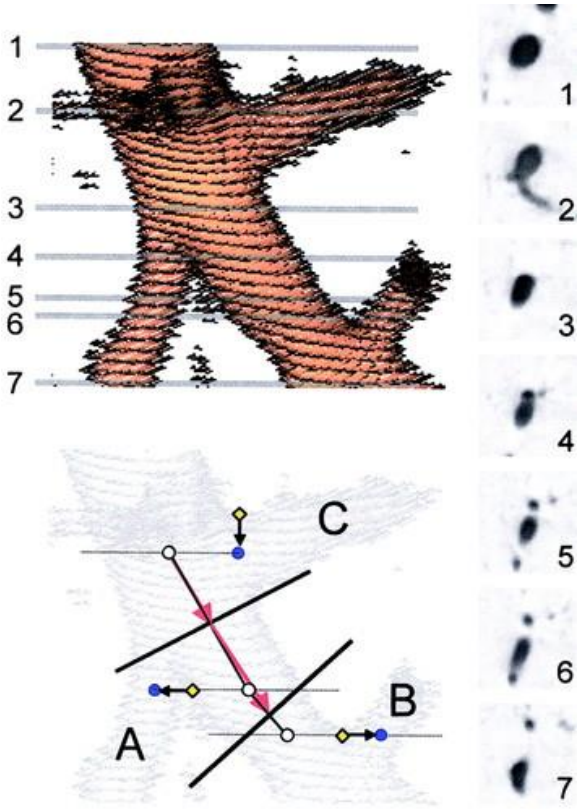

Fig. 3. Identification of vessel segments in the image volume. The numbered horizontal lines through the surface shaded rendering on the upper left designate the numbered locations of the transaxial slices on the right. The transaxial slices are used by the operator to locate bifurcation points and the central axes of trunk and branch vessel segments. This section of the tree was chosen for diagrammatic purposes because it contains all three bifurcation types encountered on traversal through a stack of transaxial slices. That is, branches like*branch B* that converge with the trunk, or like*branch A* that diverge from the trunk, or like*branch C*, that are nearly in the plane of the transaxial slices, as observed during a traversal through the stack of slices that compose the image volume. The lower left image specifies branch types, bifurcation points (gold diamonds), and line segments identified in text (see methods). The blue circles are located on the axes of the branches. The white circles are located on axes of the trunk. Planes orthogonal to the axes designated by the black lines are the planes on which the trunk diameters are measured. Red arrows are the distance measurements contributing to the cumulative distance*x*.

The two additional cases are also illustrated in Fig. 3. When the branch and trunk converged (*branch B*), so that the ellipsoids merged on progression through the slices, *z* was identified as being in the plane just before the merger. The central*x*,*y* coordinates were then recorded in the same manner as in the first case. The third case is evident when one of the vessels is oriented so nearly parallel to the transaxial slices that the lobulation indicative of a bifurcation appears elongated rather than as a distinct ellipse (e.g., *branch C* in Fig. 3).

The *z* coordinate was identified by observing the proximal intersection of the branch with the trunk, and by proceeding through the volume half the number of slices encompassing the full width of the horizontal vessel segment. The central *x*,*y*coordinates of the oblique vessel segment were identified on this plane as in *cases A* and *B*. The central*x*,*y* coordinates of the horizontal segment were placed on this same plane but on the visually interpolated edge of the oblique vessel ellipse.

Once these *x*,*y*,*z* coordinates of the main trunk (white circles in Fig. 3) and the upstream ends of the branches (blue circles in Fig. 3) were located, the upstream branch coordinates were revisited. Each branch was followed as it diverged from the trunk until the first bifurcation was reached. The downstream*x*,*y*,*z* coordinates were then identified in the same manner as described for *cases A*, *B*, and *C*. For most branches, the process ended at this first bifurcation off the main trunk. However, nine branches were designated minor trunks and followed to their respective terminations as was the main trunk.

Having identified these coordinates, the midpoints $[(x_1 + x_2)/2, (y_1 + y_2)/2, (z_1 + z_2)/2]$ of the line between consecutive trunkx_i,y_i,$z_i$coordinates and between upstream and downstream branchx_i,y_i,$z_i$coordinates were identified. Two vectors intersecting these midpoints, orthogonal to each other and to the central axis, specified an orthogonal plane through the midpoint of the central axis line segment. The thick black lines in Fig. 3, *bottom left*, represent one of each pair of these vectors. Cubic interpolation was performed to obtain the GSN values of the orthogonal slice on this plane. The vessel segment diameter was estimated from its cross-sectional image in this slice as previously described (21). The distance along a trunk was computed as the cumulative distances between consecutive midpoints, beginning at the *x*,*y*,*z* of the inlet segment.

Note that Fig. 3 represents the identification of the coordinates and central axes. The diameter measurements were made on the orthogonal slices wherein the vessel cross sections appear as circles rather than ellipses as shown previously (21). Whereas the identification of the *x*,*y*,*z*coordinates was interactive, once the coordinates were specified, the diameter measuring algorithm was automatic. One can appreciate that the orthogonal slice through the midpoint between the *case A* and *case B* bifurcations on Fig. 3 would be circular, whereas the orthogonal slice through the midpoint between*case A* and *case C* would be distorted due to the fact that the two branches come off the trunk less than a full branch diameter apart. The effect of this distortion is averaged in the vessel diameter estimate by the optimization procedure (21). These cases contribute to the apparent roughness of the taper of the trunks observed in the diameter- versus-distance plots presented in *Principal pathway parameterization*. If the trunk segment was distorted to the extent that the diameter-measuring algorithm did not converge, the next downstream trunk location was assigned two branches rather than one (the algorithmic definition of a trifurcation). The overall result was robust with regard to the operator choices. For example, as *case A* or *case B* bifurcation approaches a *case C*bifurcation, the choice of method makes little difference to the outcome. Confusion with regard to a *case A* or *case B* does not occur.

RESULTS

The data obtained was a contiguous sequence of axial segments consisting of the main trunk and nine minor trunks, and the diameter of the branch off of the main trunk associated with each segment.

Principal pathway parameterization.

The distances through the lumen from the inlet to the ends of the contiguous sequence of axial segments consisting of the main trunk and nine minor trunks are plotted on Fig. 4,*A*, *C*, and *E*. To further investigate the self-consistency of the arterial tree, we begin by observing that the diameter, *D*, vs. distance, *x*, along the main trunk has an appearance reminiscent of the following functional form

$$D(x) = D(0)(1 - x/L_{\text{tot}})^c$$

Equation 1

where $D(0)$ is an approximation to the trunk diameter at $x = 0$; L_{tot} would be the total length of the trunk if extended until $D = 0$, i.e., $D(0)/L_{tot}$ is a measure of the average taper of the entire trunk, and c is the measure of the concavity-convexity of the taper, i.e., when $c < 1$, the curvature of the taper is convex to the trunk axis, and when $c > 1$, the curvature of the taper is concave to the axis. A conceptual representation of *Eq. 1* is shown in Fig. 5.

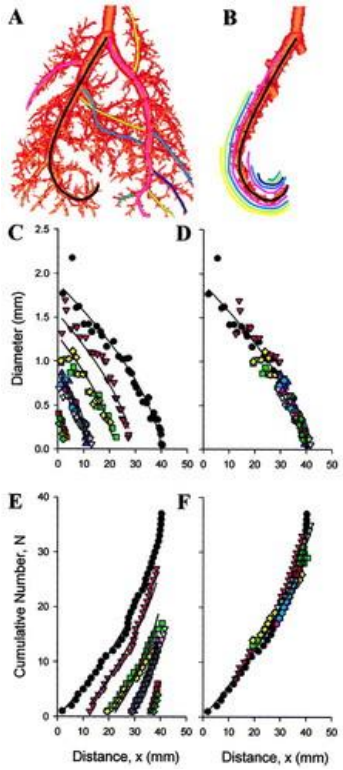

Fig. 4. *A*: same surface-shaded renderings as in Fig.1, with 10 trunks identified by colored lines. *B*: The 10 colored lines have been bent and placed along the main trunk to demonstrate diagrammatically where the minor trunks would superimpose on the main trunk. *C*: diameter (D) versus distance (x) relationships for the 10 individual trunks identified in the top images, with *Eq. 2* fit through the data. The distance, $x = 0$, is where the branch leaves the main trunk. *D*: superposition of the nine trunks on the main trunk by shifting the distance axis by s_i to the right. *E*: cumulative number of branches (N_{Br}) vs. x along the 10 trunks identified at *top*. On this graph, the branches start at their respective locations, s_i, along the main trunk. The lines are *Eq. 4* fit though the data. *F*: superposition of the 9 minor trunks on the main trunk accomplished by shifting up by n_i.

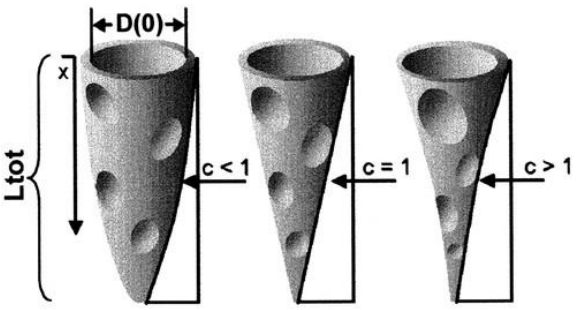

Fig. 5. Schematic representation of the parameters of *Eq.1* describing the main trunk geometry. $D(0)$, approximation to the trunk diameter at $x = 0$; L_{tot}, total length of the trunk if extended until $D = 0$; c is the measure of the concavity-convexity of the taper.

Self-consistency implies that if *Eq. 1* describes the *D* versus *x* relationship for the main trunk, then the *D* versus *x* graph of any trunk would be described by *Eq. 2*

$$D(x) = D(0)[1 - (x + s_i)/L_{tot}]^c$$

Equation 2

where $D(0)$, L_{tot}, and c would be the same for all trunks, and s_i would be the distance along the x-axis of Fig. 4*C* that an individual trunk would need to be shifted to match the equivalent distal portion of the main trunk. Thus fitting *Eq. 2* to all of the data from the 10 trunks on Fig. 4*C* simultaneously yields 12 parameters, 9 unique s_i values (s_i for the main trunk is 0) and 1 common value each for $D(0)$, L_{tot}, and c for the 10 pathways. Because of its distortion due to the cannulation, the main pulmonary artery is not included in the main trunk data set. Instead, $x = 0$ occurs at the bifurcation of the pulmonary artery, so that $D(0)$ is the *Eq. 2* approximation to the right pulmonary artery inlet diameter. The fitting of this and the subsequent equations to the data was carried out using the FMINS routine in the Matlab version 6 optimization toolbox. Because a value of $D(x)$ at $x > L_{tot}$ is not a real number (i.e., a negative number raised to the power c), *Eqs. 1* and *2* were set to 0 when $x > L_{tot}$ (or $x + s_i > L_{tot}$) occurred during this and subsequent optimizations for equations having similar form. To construct Fig. 4*D*, the data for the minor trunks were horizontally translated to the right by the distances s_i. The resulting superposition is a characteristic of self-consistency.

Another characteristic of self-consistency is that the branches off any trunk should be similarly distributed. Figure 4*E* again shows the 10 trunks, but with the number of upstream branches (N_{Br}) plotted versus x. On the left, each trunk begins at its respective s_i. The progression of the curves is again suggestive of self-consistency.

To further investigate this aspect of self-consistency of the arterial tree, we note that N_{Br} versus x along the main trunk has the appearance of the following functional form

$$N_{Br}(x) = N_{tot}\{1 - [1 - (x/L_{tot})]\}^b$$

Equation 3

where N_{tot} is an approximation to the total number of branches off the main trunk, i.e., N_{tot}/L_{tot} is a measure of the average number of branches per unit length, and b is the measure of how the branches are distributed along the length, i.e., when b is >1, the number of branches per unit length increases with x and when b is <1, the number of branches per unit length decreases with x. Thus a change in N_{tot}/L_{tot} would reflect a change in branch density, whereas a change in b would distinguish the large versus small vessel contribution to such a change.

Self-consistency implies that if *Eq. 3* describes N_{Br} versus x relationship for the main trunk, then the number versus x graph of any trunk would be fit by *Eq. 4*

$$N_{Br}(x) = N_{tot}\{1 - [1 - (x + s_i)/L_{tot}]\}^b - n_i$$

Equation 4

where N_{tot} and b would be the same for all trunks and n_i would be the number of branches an individual trunk would need to be shifted to match the equivalent distal portion of the main trunk. Thus, fitting *Eq.4* to all of the data from the 10 trunks shown in Fig.4*E*, simultaneously yields 11 parameters, 9 unique n_i values (n_i for the main trunk is 0) and 1 common value each for N_{tot}, and b for the 10 pathways. Because a value of $x > L_{tot}$ is not a real

number, $x > L_{tot}$ (or$x + s_i > L_{tot}$) were ignored if they occurred during this and subsequent optimizations for equations having similar form. The resulting superposition, in Fig. 4*F*, along with that in Fig.4*D*, is the basis of the following parameterization of the tree structure.

Under the assumption of self-consistency, only the dimensions of the main trunk and the diameters of its immediate branches need to be measured to fully characterize the tree structure. With *Eq.1* as the representation of the main trunk diameter versus distance relationship, *Eq. 5* can represent the diameters,D_{Br}, of the vessel segments branching off the main trunk at *x*

$$D_{Br}(x) = D_{Br}(0)(1 - x/L_{tot})^c + \varphi$$

Equation 5

where $D_{Br}(0)$ is an approximation to the diameter of the first branch off the main trunk (the left pulmonary artery), and, assuming self-consistency,$D_{Br}(0)/D(0)$ is an average ratio of branch-to-trunk diameters. Although represented by a continuous function, the branches are actually placed only at the number,N_{tot}, of discrete locations along the main trunk, and their diameters vary with *x* proportionately much more than the main trunk diameter. The ϕ is a variable diameter increment reflecting this heterogeneity of the branch diameter along the principle pathway. Figure 6 represents an entire principle pathway data set with *Eqs. 1* and *5* fit simultaneously with four free parameters:$D(0)$, $D_{Br}(0)$,L_{tot}, and *c*, and with ϕ = 0. ϕ was then represented by a coefficient of variation (CV_{Br}) obtained from the variance in the measured branch diameter around the fitted *Eqs. 1* and *5*, namely

$$CV_{Br} = \sqrt{\frac{\left(\frac{D_{Br}\text{data} - D_{Br}\text{fit}}{D_{Br}\text{fit}}\right)^2 - \left(\frac{D\text{data} - D\text{fit}}{D\text{fit}}\right)^2}{N - 4}}$$

Equation 6

where data refers to the measured value and fit refers to the value predicted by the fit of *Eq. 5* to the data for each of the N_{tot} branches along the principal pathway. The rationale behind *Eq. 6* is the concept that there is an underlying smooth taper to the main trunk that can be represented by*Eq. 1*, and that the variability in measured data about the fitted line reflects the irregular distortion of the smooth taper near bifurcations as well as errors in the diameter estimates. Assuming that these sources of variance also exist in the branch diameter data, subtracting the variance about the fit to *Eq. 1* from that around *Eq. 5* provides an approximation to the variance in the branch diameters due to the heterogeneity in the branch-to-trunk diameter ratio.

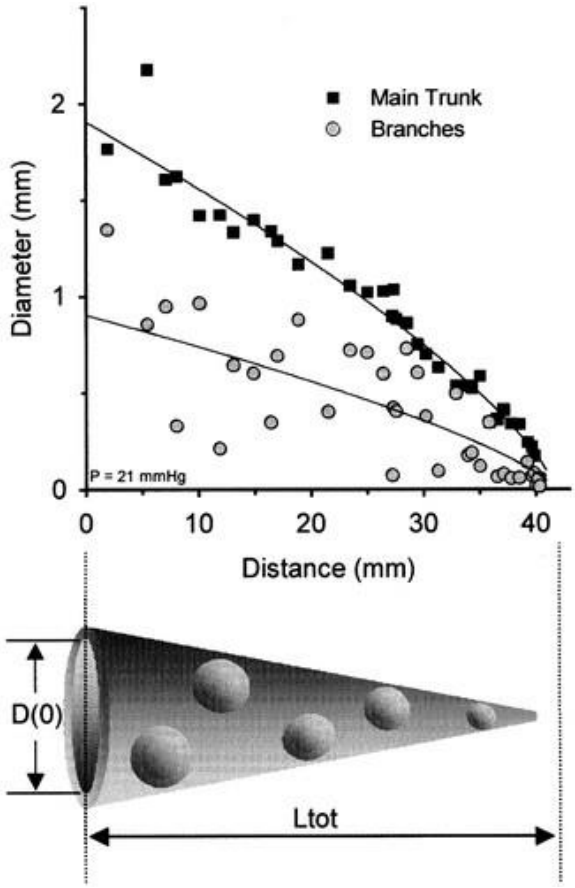

Fig. 6. Principal pathway data including the main trunk diameter at *x* from the bifurcation of the main pulmonary artery and the diameters and *x* locations of the branches off of the main trunk. Data are from images obtained at an arterial pressure of 21 mmHg. Below the *x*-axis is another schematic representation of the main trunk to emphasize the concept that the principal pathway is a tapered tube with branches, represented in this depiction as depressions or scars where the branches have been broken off.

From *Eqs. 1, 3*, and *6*, the parameter vector summarizing the tree morphometry at a given vascular pressure would be [$D(0)$, $D_{Br}(0)$,L_{tot}, N_{tot}, c,b, CV_{Br}]. However, as illustrated in Fig. 7, the vessel diameters are also a function of vascular pressure, which over the pressure range studied can be approximated by *Eq. 7* (1, 39, 42)

$$D(x,P) = D(x,0)(1+\alpha P)$$

Equation 7

where α is a distensibility coefficient, namely, the fractional change in diameter per unit change in pressure. Assuming that α is diameter independent (1, 21), *Eqs. 2* and *4* can be written as

$$D(x,P) = D(0,0)(1+\alpha P)(1-x/L_{tot})^{c}$$

Equation 8

and

$$D_{Br}(x,P) = D_{Br}(0,0)(1+\alpha P)(1-x/L_{tot})^{c} + \varphi$$

Equation 9

Thus the [$D(0,0)$, $D_{Br}(0,0)$,L_{tot}, N_{tot}, c,b, CV_{Br}, α] vector can be obtained by fitting *Eqs. 8*, *9*, and *3* to all of the principal pathway data obtained over the entire pressure range studied. The approach was to first simultaneously fit *Eqs. 8* and *9* to the $D(x,P)$ and$D_{Br}(x,P)$. The two surfaces representing this fit are shown in Fig.8. Then the $L_{tot}$was used as an input to *Eq. 3*, which was then fit to the$N_{Br}(x)$ data as shown in Fig.9 to obtain the estimates ofN_{tot} and b for all pressures simultaneously. Although a slight increase inL_{tot} with increasing pressure can be observed in Fig. 9 it was not considered to be of sufficient magnitude to warrant consideration in the model expressions. We suspect that it is mainly due to a small stretching of the vertically oriented lungs as the lung weight increased with increasing mass of PFOB. In any case, there is no evidence for a substantial effect of intravascular pressure on vessel lengths. The parameter values obtained in this manner for the lung studied are as follows: $D(0,0)$ = 1.34 mm,$D_{Br}(0,0)$ = 0.610 mm,L_{tot} = 41.2 mm,N_{tot} = 37, c = 0.695,b = 1.67, CV_{Br} = 54.6%, and α = 2.25% mmHg

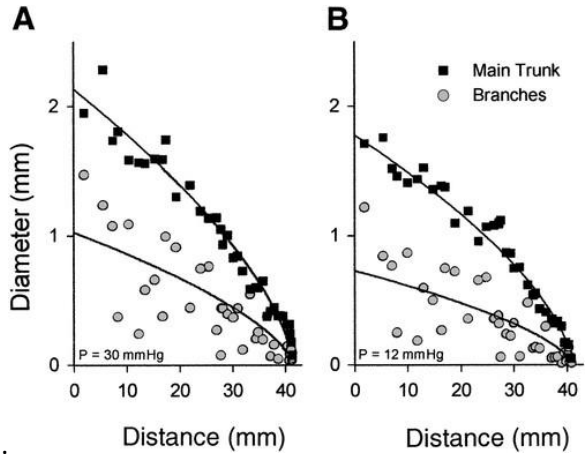

.

Fig. 7. Principal pathway data similar to Fig. 6, but from images obtained with the arterial pressure set at 30 mmHg (*A*) and 12 mmHg (*B*) to demonstrate vessel distensibility.

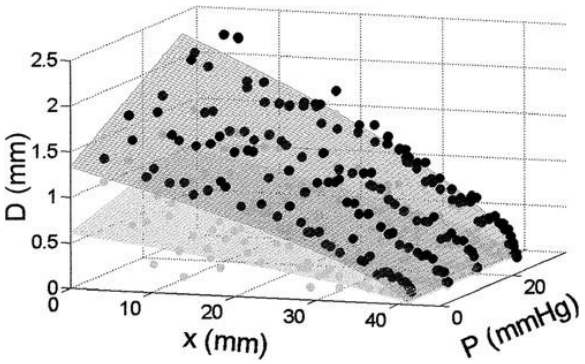

Fig. 8. The entire principal pathway diameter versus distance data set from the images obtained at all pressures. The two surfaces are fit simultaneously from *Eqs. 8* and *9* to the entire data set.

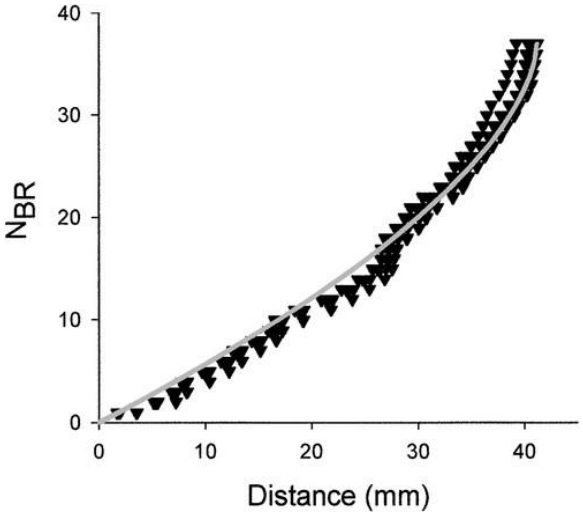

Fig. 9. Entire N_{Br} vs. *x* data set from the images obtained at all pressures. The line is *Eq.3* fit simultaneously to the entire data set.

One objective of this study was to develop a method for morphometric analysis with high enough throughput that comparisons can be made between lungs and between groups of lungs in future studies. We envision this parameter vector to be the basis of such comparisons. In addition, elements of the parameter vector can also be used to extrapolate the relatively small number of measurements made to an entire tree structure. An example approach would be as follows. The first step is to determine the distances between branches,$L(N_{Br})$, in the model tree using*Eq. 10*

$$L(N_{\mathrm{Br}}) = L_{\mathrm{tot}}\{[1-(1-(N_{\mathrm{Br}}/N_{\mathrm{tot}})]^{1/b}\}$$

Equation 10

$$-\{1-[1-[(N_{\mathrm{Br}}-1)/N_{\mathrm{tot}})]^{1/b}]\}$$

Then the branch *x* positions along the trunk are identified from the cumulative$L(N_{Br})$. In a self-consistent tree, the main trunk diameter must decrease monotonically from the inlet. Therefore, the next step is to calculate the model main trunk diameter using *Eq. 8* for the particular pressure chosen for the model. The branch diameters (the average from the five pressures for each branch normalized to the *Eq. 8* trunk surface) can then be used to determine the model branch diameters. This is done by reassigning each branch diameter the trunk diameter closest to the mean branch diameter, unless the branch diameter was smaller than the smallest measured trunk diameter. In the latter case, the trunk was extended along the *Eq. 1* line to include the branch diameter. An entire tree down to the resolution of the image data can then be constructed using the self-consistency recursion relationship that results from all vessels down stream from a givenN_{Br} having the same dimensions. As with any model specified by a smaller number of parameters than the dimensions of the real system, the tree constructed is a stereotypical approximation to the real tree. However, it retains representations of asymmetry and heterogeneity missing from some morphometric synopses (6) and in a way that can provide input to a computationally efficient hemodynamic model (9). This model tree is depicted in Fig. 10 in the format of Figs. 6 and 7 except that lines representing the minor trunks and their immediate branches have been added to give an impression as to how the principal pathway data are extrapolated to the entire tree. The entire tree would be represented by many more lines because the branches off of the minor trunks become minor trunks and so on.

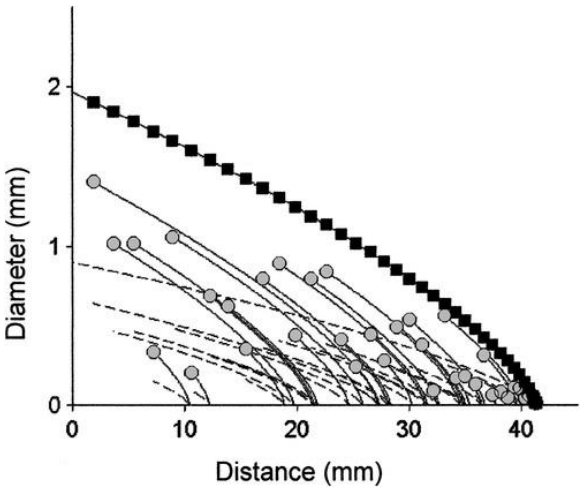

Fig. 10. Self-consistent model tree, for a pressure of 21 mmHg, constructed from the parameter vector obtained from the *Eq.8* and *9* fit to the surfaces in Fig. 8 and *Eq. 3* fit to the data in Fig. 9. Model trunk diameters (■) at the *x* locations correspond to each branch diameter (●). The solid lines are the individual trunk diameter versus *x*relationships for the main trunk and those minor trunks beginning at a branch off the main trunk. Dashed lines are the *Eq. 9* for each minor trunk.

DISCUSSION

The results suggest that the rat pulmonary arterial tree is self-consistent and conducive to principal pathway analysis. This property may be useful for summarizing the pulmonary arterial morphometric data available in the three-dimensional volume reconstruction of the lung. A practical consequence of self-consistency is that it minimizes the number of measurements needed to characterize the complex tree structure consisting of thousands of vessel segments. This will be important, at least until completely automated image segmentation methods become available. Another practical consequence is that self-consistency lends itself to a computationally efficient means of evaluating the hemodynamic impact of changes in the structure (9).

The expectation is that the parameter vector obtained as described will serve three interrelated purposes as indicated in the introduction. One is to provide a basis for comparing the lumenal morphometry of pulmonary arterial trees in animals exposed to different remodeling stimuli and to interventions directed at putative mechanisms involved in the remodeling. Also, if any element of the vector is found to exhibit differential susceptibility to a particular remodeling stimulus in a specific rat strain, it may be a useful phenotype for quantitative trait localization by genetic linkage analysis (7). A third purpose is as input to mathematical models relating pulmonary vascular structure and function in normal and remodeled pulmonary arterial systems (2, 6, 42). In this regard, the parameter vector can be translated into a structure amenable to hemodynamic modeling similar in concept to the airway modeling of Fredberg and Hoenig (9, 10). The recursion relationships that result from self-consistency (alluded to in Fig. 10) provide computational efficiency for large heterogeneous asymmetrical structures. The objective of that kind of modeling would be to determine how changes in the morphometry and vessel mechanics, revealed by changes in the parameter vector, contribute to the changes in function, e.g., pulmonary hypertension, abnormal distributions of flow, shear stress, etc.

We chose the rat lung for this developmental study because of its history of use in studies of pulmonary vascular remodeling (28,29, 36), because of its increasing importance in genetic studies (7, 17, 31, 34), and because a small lung takes advantage of the geometric magnification possible with microfocal imaging. For the combination of image-acquisition procedures in the present study, the smallest arteries for which diameters were confidently measured were ~50 μm in diameter (21). The diameters of terminal pulmonary arteries, i.e.,

arteries connecting directly to capillaries, have reported to range from ~13 to 30 μm in diameter in various studies and species (5), which is just beyond the resolution in the present study. Improvements in computational capacity to take advantage of the higher resolution capabilities of the detector system and the use of volume of interest reconstruction (23, 30) to allow for higher geometric magnification than in the full lung reconstruction used in the present study, are examples of feasible enhancements for future development.

The algorithms developed to quantify the 3D image volumes are partially automated (containing some interactive steps). Whereas advances are being made in the field of vessel segmentation in micro CT images (11, 37) that may be applicable to lung images in the future, the method described for locating a bifurcation seems to produce a satisfactory result and can be easily and robustly implemented by the operator. Each branch is associated with a segment of the trunk, but no attempt was made to establish a specific location along the segment. Other approaches are possible. For example, Wood et al. (38) defined the bifurcation (branch) point as the intersection of the central axes of the parent and two daughters, and they developed a means for identifying that point. One criterion for judging the value of adding such a method in the future might be the sensitivity of a hemodynamic model to how the branches are distributed along the total length of the principle pathway. Given the relative sensitivity of the pressure-flow relationship to the diameter versus the length of a vessel segment, one might anticipate that the sensitivity will not be great. In fact, the robustness with regard to individual length variations may be one of the reasons that evolutionary forces have not done more to narrow the wide variation in segment length-to-diameter ratio in the pulmonary vascular bed (35), or in other vascular beds (35, 41). With the approach taken, cumulative distance along a pathway, which is insensitive to the definition of the length of an individual segment, is given primacy.

The functional forms fit to the data in the present study were chosen because they represent major trends in the data with a minimum number of parameters, the forms are similar to those resulting from a previous symmetrical tree analysis (5), and the parameters have clear interpretations with respect to the shape of the principal pathway (Figs. 5 and 6). It remains to be seen whether this parameter vector has the flexibility to represent all of the systematic and important variations that might occur. However, it might be considered a nested version of a higher dimensional model that might need to be constructed to include such variations. For example, the representation of the vascular distensibility by a single diameter-independent parameter may need adjustment if the diameter-dependent remodeling of the vessel walls, which has been reported in rats exposed to various stimuli (22, 26, 28), also results in diameter-dependent distensiblity. It may be surprising that the distensibility can be represented by a single parameter even in the normal rat. This uniformity has been observed previously for the rat (21) and other species (1), and it can be appreciated by observing the proportionate changes in the diameters of the trunk and branches along the trunk length in Fig. 7 as well as in the surface fit in Fig. 8.

Although the rat was used in the present study, it seems likely that other mammalian species will have self-consistent pulmonary arterial trees. The morphometric analysis of Liu et al. (24) on the portions of the dog pulmonary arterial tree having dimensions accessible in whole animal CT scans would appear to support that contention. Likewise, insofar as the arterial tree follows the airway structure, airway self-consistency (9, 15) would predict arterial self-consistency. When the entire pulmonary arterial tree is in the field of view, species differences in gross structure are generally discernible (6). One of the distinguishing features at the whole tree level of observation is the degree to which the structure is dominated by a branching pattern wherein the two daughter branches at a bifurcation are more nearly equal in diameter [dichotomous (4, 14)] or a pattern wherein one of the two daughters tends to be much smaller than the parent [monopodial (4, 14)]. These are sometimes referred to as maple tree versus pine tree-like structures, respectively. The latter has a more obvious main trunk than the former. Application of the principal pathway analysis does not imply a predominantly monopodial branching pattern. Such a pattern may make it easier to decide which pathway to follow at a

bifurcation. However, if two equal branches were ever encountered (an uncommon event even in the most dicotomously branching trees), according to the self-consistency concept, following either pathway would produce the same result. As a related point, gross differences between species that can be observed at low magnification tend to disappear at high magnification (6). This is probably related to the fact that the functional respiratory units also tend to have similar species-independent structures and the fact that the arteries eventually have to hook up to the capillaries that are essentially all one size. Self-consistency, as we have used the term, implies that, having traversed the longest pathway through the tree, the structure downstream of any vessel of a given diameter is known. Thus, using local diameter as the landmark, self-consistency requires a continuous taper along each pathway (i.e., that the daughter branches at a bifurcation are smaller than the parent). This self-consistency does not extend into the capillary bed because local capillary diameter provides no information about how much of the capillary bed lies downstream from that location. This self-consistency does not require the scale independence of a fractal structure, but it does imply that, as one progresses through the tree, the local diameter specifies (in a statistical sense) the downstream structure. A self-consistent tree structure has attributes of a fractal in entreating simplified mathematical representation of the complex structure. Whereas a fractal tree can be self-consistent, self-consistency does not require scale independence. However, the transformation imposed by certain ordering schemes can reveal fractal relationships in the transformation space that are not necessarily evident in the direct appearance of the structure (6, 18, 41).

In conclusion, the results demonstrate self-consistency in the rat pulmonary arterial tree. An approach for exploiting this property is presented. The approach may be one way that high spatial resolution volumetric X-ray CT can contribute to the information required for understanding normal pulmonary arterial structure-function relationships and how these relationships are affected by pulmonary vascular remodeling associated with pulmonary vascular development, adaptations to environmental stress, or disease.

This study was supported by National Heart, Lung, and Blood Institute Grant HL-19298, The Whitaker Foundation, The W. M. Keck Foundation, The Falk Medical Trust, and the Department of Veterans' Affairs.

FOOTNOTES

- Address for reprint requests and other correspondence: C. A. Dawson, Research Service 151, Zablocki Veterans Affairs Medical Center, 5000 W. National Ave., Milwaukee, WI 53295 (E-mail: cdawson@mcw.edu).

- The costs of publication of this article were defrayed in part by the payment of page charges. The article must therefore be hereby marked "*advertisement*" in accordance with 18 U.S.C. Section 1734 solely to indicate this fact.

REFERENCES

1 Al-tinawi A, Madden JA, Dawson CA, Linehan JH, Harder DR, Rickaby DA. *Distensibility of Small Arteries of the Dog Lung*. J Appl Physiol *71* 199117141722

2 Bassingthwaighte, JB. *Strategies for the Physiome Project*. Ann Biomed Eng *28* 200010431058

3 Bennett SH, Eldridge MW, Zaghi D, Zaghi SE, Milstein JM, and Goetzman BW. *Form and Function of Fetal Neonatal Pulmonary Arterial Bifurcations.* Am J Physiol Heart Circ Physiol *279* 2000H3047H3057

4 Cumming C, Henderson R, Horsfield K, Singhai SS. *The Functional Morphology of the Pulmonary Circulation*. The Pulmonary Circulation and Interstitial Space, Fishman AP, Hecht HH.1969327340Univ. of Chicago PressChicago, IL

5 Dawson CA, Krenz GS, Karau KL, Haworth ST, Hanger CC, Linehan, JH. *Structure-Function Relationships in the Pulmonary Arterial Tree.* J Appl Physiol *86* 1999569583

6 Dawson CD, Krenz GS, Linehan JH. *Complexity and Structure-Function Relationships in the Pulmonary Arterial Tree*. Lung Biology in Health and Disease, Complexity in Structure and Function of the Lung**,** Hlastala MP, Robertson HT.1998DekkerNew York, chapt. 13, p. 401–427.
7 Dumas PM, Granados Dawson C, Jacob H. *Genetic Dissection of Pulmonary Hypertension in Fawn-Hooded Rats by Chromosomal Substitution* (Abstract).FASEB J *15* 2001A857
8 Feldkamp LA, Davis LC, Kress JW. *Practical Cone-Beam Algorithm*. J Opt Soc Am A *1* 1984612619
9 Fredberg JJ. *Airway Dynamics: Recursiveness, Randomness, and Reciprocity in Linear System Simulation and Parameter Estimation***.** Lung Biology in Health and Disease, Respiratory Physiology: An Analytical Approach, Chang MK, Paiva M.1989DekkerNew York, chapt. 4, p. 167–194.
10 Fredberg JJ, Hoenig A. *Mechanical Response of the Lungs at High Frequencies*. J Biomech Eng *100* 19785766
11 Herold CJ, Wetzel RC, Robotham JL, Herold SM, Zerhounui, A. *Acute Effects of Increased Intravascular Volume and Hypoxia on the Pulmonary Circulation: Assessment with High Resolution CT1.* Radiology *183* 1992655662
12 Higgins WE, Spyra WJT, Karwoski RA, Ritman EL. *System for Analyzing High Resolution Three-Dimensional Coronary Angiograms*. IEEE Trans Med Imaging *15* 1996377385
13 Horsfield K. *Morphometry of Small Pulmonary Arteries in Man*. Circ Res *42* 1978593597
14 Horsfield K, Cumming G. *Morphology of the Bronchial Tree in Man*. J Appl Physiol *24* 1968373383
15 Horsfield K, Kemp W, Phillips S. *An Asymmetrical Model of the Airways of the Dog Lung*. J Appl Physiol *52* 19822126
16 Huang W, Yen RT, McLaurine M, Bledsoe G. *Morphometry of the Human Pulmonary Vasculature.* J Appl Physiol *81* 199621232133
17 Jacob HJ. *Functional Genomics and Rat Models*. Genome Res *9* 199910131016
18 Jiang Z, Kassab GS, Fung YC. *Diameter-Defined Strahler System and Connectivity Matrix of the Pulmonary Arterial Tree*. J Appl Physiol *76* 1994882892
19 Johnson RH, Hu H, Haworth ST, Cho PS, Dawson CA, Linehan JH. *Feldkamp and Circle-and-Line Cone-Beam Reconstruction for 3D Micro-CT of Vascular Networks*. Phys Med Biol *43* 1998929940
20 Jorgensen SM, Demirkaya O, Ritman EL. *Three-Dimensional Imaging of Vasculature and Parenchmyma in Intact Rodent Organs with X-ray Micro-CT*. Am J Physiol Heart Circ Physiol *275* 1998H1103H1114
21 Karau KL, Johnson RH, Molthen RC, Dhyani AH, Haworth ST, Hanger CC, Roerig DL, Dawson CA. *Microfocal X-ray CT Imaging and Pulmonary Arterial Distensibility in Excised Rat Lungs*. Am J Physiol Heart Circ Physiol *281* 200114471457
22 Kay JM, Suyama KL, Keane PM. *Failure to Show Decrease in Small Pulmonary Blood Vessels in Rats with Experimental Pulmonary Hypertension*.Thorax *37* 1982927930
23 Lewitt RM. *Processing of Incomplete Measurement Data in Computed Tomography*. Med Phys *6* 1979412417
24 Liu YH, Hoffman EA, Ritman EL. *Measurment of Three-Dimensional Anatomy and Function of Pulmonary Arteries with High Speed X-ray Computed Tomography*. Invest Radiol *22* 19872836
25 Liu YH, Ritman EL. *Branching Pattern of Pulmonary Arterial Tree in Anesthetized Dogs*. J Biomech Eng *108* 1986289293
26 Meyrick B, Gamble W, Reid L. *Development of Crotalaria Pulmonary Hypertension: Hemodynamic and Structural Study*. Am J Physiol Heart Circ Physiol *239* 1980H692H702
27 Nadeau JH, Singer JB, Matin A, Lander ES. *Analysing Complex Genetic Traits with Chromosome Substitution Strains*. Nat Genet *24* 2000221225
28 Rabinovitch M, Gamble W, Nadas AS, Miettinen OS, Reid L. *Rat Pulmonary Circulation After Chronic Hypoxia: Hemodynamics and Structural Features.* Am J Physiol Heart Circ Physiol *236* 1979H818H827
29 Riley DJ, Thakker-Varia S, Poiani GJ, Tozzi CA. *Vascular Remodeling.* The Lung: Scientific Foundations 2nd ed., Crystal RG, West JB, Barnes PJ, Weibel ER.199715891597Lippincott-RavenPhiladelphia, PA
30 Ritman EL, Dunsmuir JH, Faridani A, Finch DV, Smith KT, Thomas PJ. *Local Reconstruction Applied to X-Ray Microtomography*. IMA Volumes in Mathematics and in Applications, Inverse Problems in Wave Propagation**.***90* 1996443452Springer-VerlagNew York

31 Sato K, Webb S, Tucker A, Rabinovitch M, O'Brien RF, McMurtry IF, Stelzner TJ. *Factors Influencing the Idiopatic Development of Pulmonary Hypertension in the Fawn Hooded Rat*. Am Rev Respir Dis *145* 1992793797
32 Shepp LA, Logan BF. *The Fourier Reconstruction of a Head Section*. IEEE Trans Nucl Sci *21* 19792142
33 Singhal S, Henderson R, Horsfield K, Harding K, Cumming G. *Morphometry of the Human Pulmonary Arterial Tree*. Circ Res *33* 1973190197
34 Stelzner T, Hofmann TA, Brown D, Deng A, Jacob HJ. *Genetic Determinants of Pulmonary Hypertension in Fawn-Hooded Rats*. Chest *111, Suppl*199796S
35 Suwa N, Niwa T, Fukasawa H, Sasaki Y. *Estimation of Intravascular Blood Pressure Gradient by Mathematical Analysis of Arterial Casts*. Tohoku J Exp Med *79* 1963168198
36 Voelkel NF, Tuder RM. *Hypoxia-Induced Pulmonary Vascular Remodeling: A Model for What Human Disease?* J Clin Invest *106* 2000733738
37 Wan SY, Kiraly AP, Ritman EL, Higgins WE. *Extraction of the Hepatic Vasculature in Rats Using 3-D Micro-CT Images*. IEEE Trans Med Imaging *19* 2000964971
38 Wood SA, Zerhouni EA, Hoford JD, Hoffman EA, Mitzner W. *Measurement of Three-Dimensional Lung Tree Structures by Using Computed Tomography*. J Appl Physiol *79* 199516871697
39 Yen RT, Fung YC, Bingham N. *Elasticity of Small Pulmonary Arteries in the Cat*. J Biomed Eng *102* 1980170177
40 Yen RT, Zhuang FY, Fung YC, Ho HH, Tremer H, Sobin SS. *Morphometry of Cat's Pulmonary Arterial Tree*. J Biomech Eng *106* 1984131136
41 Zamir M. *On Fractal Properties of Arterial Trees.* J Theor Biol *197* 1999517526
42 Zhuang FY, Fung YC, Yen RT. *Analysis of Blood Flow in Cat's Lung with Detailed Anatomical and Elasticity Data.* J Appl Physiol *55* 198313411348